



Electrocatalysis of oxygen reduction at electrodeposited molybdenum phosphate-based films

Gisela C. Luque, José L. Fernández*

Programa de Electroquímica Aplicada e Ingeniería Electroquímica (PRELINE), Facultad de Ingeniería Química, Universidad Nacional del Litoral, Santiago del Estero 2829 (S3000AOM), Santa Fe (Santa Fe), Argentina

ARTICLE INFO

Article history:

Received 2 September 2011
Received in revised form
29 November 2011
Accepted 30 November 2011
Available online 8 December 2011

Keywords:

Oxygen reduction
Molybdenum phosphate
Electrocatalysis
Pt-free cathodes

ABSTRACT

This work reports an electrode material containing molybdenum phosphate that shows a very interesting behavior as an electrocatalyst for the reduction of oxygen to water (ORR) in acid medium. The material is electrodeposited on a glassy carbon electrode from a solution of Mo(VI) and Co(II) in phosphate buffer at pH=7. Cobalt is required to obtain a compact and uniform film. It is a non-crystalline solid conformed by metal oxide and phosphate groups that, according to XPS analysis, contains mostly Mo(VI) and a small fraction of Mo(V). Even though most of the Co-containing phase dissolves in acid, the film keeps its integrity and shows stable ORR activity in acid at very low overpotentials (from -0.3 V). The observed current density reaches a very small limiting value ($\sim 2 \mu\text{A cm}^{-2}$) that is independent of the mass-transport conditions and could be associated to the small fraction of Mo(V) centers that function as ORR active sites. Although the film is thermally stable up to temperatures of 400°C , by heating the material at temperatures above 100°C it loses its unusual ORR activity due to the complete oxidation of Mo(V) to Mo(VI).

© 2011 Elsevier B.V. All rights reserved.

1. Introduction

The search of alternative platinum-free electrocatalysts for energy-conversion devices (i.e. fuel cells, solar electrolyzers) has led to the discovery and development of novel electrode materials. The cathode of the proton exchange membrane fuel cells (PEMFC) is, by far, one of the research topics that concentrate most of the work in this area due to the cost and poor performance of present Pt-based oxygen reduction (ORR) catalysts [1–3]. There are a few examples of ORR electrocatalysts free of noble metals that are in a fairly advanced development stage close to implementation in PEMFC cathodes [4]. The evolution of the performance of all these materials along time is clearly observed from the first studies that showed their high potentiality. Thus for example, today one of the most promising materials is based on composites of transition metals (Fe, Co) and N-containing carbon-based structures [5,6], which were developed from the early works done on Co phthalocyanine by Jasinski [7]. Other potentially scalable ORR catalysts are the metal chalcogenides first reported by Alonso Vante et al. [8], and the films based on transition metal hexacyanometallates developed by Itaya et al. [9].

A type of material that has attracted much interest from catalysis in the last years is conformed by a growing variety of metal phosphates. A considerable number of transition metals are able to form one-, two- or three-dimensional framework materials built from the linkage of phosphate and metal oxide units [10]. These phosphate-based framework solids are a class of material that remains scarcely explored in electrocatalysis in spite of the great potentiality of these structures. For example, in an attempt to develop more efficient ORR electrocatalysts, platinum was supported on iron phosphate films by Bouwman et al. [11] and on Keggin type heteropolyacids of molybdenum and tungsten by Chojak et al. [12]. A recent example where a phosphate-based film was used as an electrocatalyst by itself was reported by Kanan and Nocera [13]. They performed the electro-synthesis and evaluation of conductive films based on cobalt polyphosphates that functioned as electrocatalysts for oxygen evolution in neutral media [13,14]. Similarly, phosphate-based films should work as ORR catalysts in acid as long as they could resist the highly acid environment of the PEMFC. On this sense, molybdenum-based phosphates [10,15] constitute an interesting group of materials for this application. This transition metal has already been the object of various studies in electrocatalysis, particularly for reduction reactions [16,17]. The interest on Mo is mainly driven for its ability to adopt varied oxidation states from +3 to +6, and to form mixed valence oxides that are conductive and stable in acid environments [18]. A great variety of Mo-based structures that combine the linkage of tetrahedral phosphate and octahedral oxide groups (MoPOs) was synthesized

* Corresponding author. Tel.: +54 342 4571164x2519;
fax: +54 342 4571164x2535.
E-mail address: jlfernand@fiq.unl.edu.ar (J.L. Fernández).

based on the rich chemistry of Mo(V) [10,15]. These MoPOs extend from zero-dimensional (0D) structures that are based on multinuclear Mo–O clusters to 3D open-framework solids synthesized by hydrothermal and high-temperature methods. These include 1D polymers and 2D layered materials, and usually involve the participation of other transition metals in addition to an alkali or organic cation [10]. Some of these compounds have shown good conductivity and are stable in acid media [19]. Taking into account the promising properties of this type of material and the lack of information on its electrocatalytic behavior, this work undertakes the development of MoPO-modified electrodes for ORR studies. In particular, a method is developed for the electro-synthesis of compact films based on MoPOs containing a second transition metal, in this case Co, and incorporating potassium as charge compensating cation (K–MoCoPO). The ORR electrocatalytic activity and stability of these films in acid are evaluated.

2. Experimental

2.1. Methods and instrumentation

2.1.1. Electrochemical experiments

Potentiostatic electrodeposition, cyclic voltammetry and potentiostatic steady-state polarization curves were performed on rotating disk electrodes (RDE) using a potentiostat Heka PG340 and a Radiometer-Copenhagen EDI10000 motor-RDE holder controlled by a Tachyprocesseur speed control unit. All electrochemical measurements were carried out in standard three-electrode cells at room temperature ($\sim 25^\circ\text{C}$).

2.1.2. Microscopic, spectroscopic and thermal characterizations

The film morphology was examined by optical microscopy, AFM and SEM, while the film composition was analyzed by energy dispersive X-ray spectroscopy (EDX), XPS, XRD and FTIR. The optical microscope was a Nikon model Optiphot. The AFM images were measured in dynamic mode using an Agilent 5400 Scanning Probe Microscope. A Zeiss SUPRA40 FEG-SEM and a JEOL JSM-35C SEM equipped with an EDAX energy dispersive spectrometer were used for acquisition of SEM images and EDX elemental microanalysis, respectively. The XPS analyses were performed using a SPECS XPS/UPS/AES system, with a Mg/Al dual X-Ray source and a hemispherical analyzer PHOIBOS 150 in FAT mode. For XRD and FTIR measurements the film was electrodeposited for 12 h, scrapped out of the glassy carbon support, and ground in an Agate mortar. This procedure was repeated several times until enough powdered sample was obtained. XRD patterns were measured in a Shimadzu XD-D1 spectrometer and FTIR spectra were recorded on powder samples supported in KBr pellets using a Shimadzu IRPrestige-21 interferometer. Thermogravimetric analysis (TGA) and thermal treatments of the films were performed in a thermobalance Mettler-Toledo TGA/SDTA851e.

2.2. Chemicals and materials

2.2.1. Electrodes

A glassy carbon (GC) RDE (3 mm diameter) was fabricated by sealing a glassy carbon rod (Alfa Aesar) in the center of a cylindrical Teflon shaft and further polishing with a sequence of unused sandpapers and alumina powder. Each time before utilization, the RDE was polished in this way and cleaned using an ultrasonic cleaner. For certain electrodes that were subjected to thermal treatments or UHV analysis (SEM, EDX, XPS), the RDE were fabricated from a glassy carbon plate (Alfa Aesar, 1 mm thickness) in such a way that the plates were removed from the Teflon shafts after film deposition. A calomel reference electrode in KCl(sat) (SCE) and a reversible hydrogen electrode prepared in situ (RHE) were used as reference

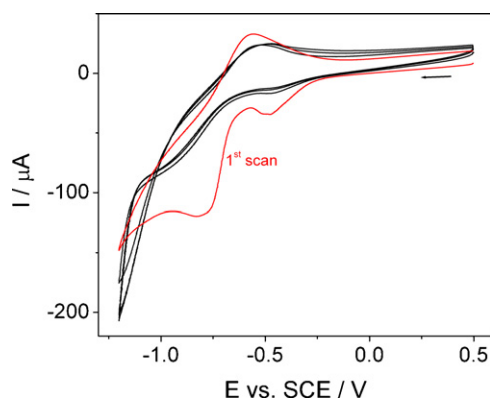


Fig. 1. Cyclic voltammogram of a glassy carbon RDE (1500 rpm) in 0.1 M potassium phosphate buffer (pH = 7) containing 0.07 M Mo(VI) and 0.001 M Co(II). Scan rate: 50 mV s^{-1} .

electrodes in electrodepositions and ORR evaluations, respectively. Large area gold wires were used as counter-electrodes.

2.2.2. Chemicals

Phosphate buffer solutions (pH=7) were prepared from dibasic potassium phosphate (K_2HPO_4 , Merck) and phosphoric acid 85 wt.% (H_3PO_4 , Cicarelli). Ammonium heptamolybdate tetrahydrate ($(\text{NH}_4)_6\text{Mo}_7\text{O}_{24}\cdot 4\text{H}_2\text{O}$, Aldrich) and cobalt sulfate heptahydrate ($\text{CoSO}_4\cdot 7\text{H}_2\text{O}$, Carlo Erba), were used as sources of Mo(VI) and Co(II) in the electrodeposition solutions. For electrocatalytic evaluations, sulfuric acid 95–97 wt.% (H_2SO_4 , Merck), hydrogen peroxide 30 wt.% (H_2O_2 , Cicarelli) and research grade gases (O_2 and N_2 99.999%, Indura) were used. Water employed in all experiments was deionized with an exchange resin, doubly distilled, and filtered with a Purelab purifier (Elga Labwater, resistivity $\geq 18.2\text{ M}\Omega\text{ cm}$).

3. Results and discussion

3.1. Electrodeposition of K–MoCoPO films

3.1.1. Voltammetry of glassy carbon in Mo(VI)–Co(II) neutral solution

Fig. 1 shows the cyclic voltammogram (CVs) of a polished GC RDE ($\omega = 1500\text{ rpm}$) in 0.1 M potassium phosphate buffer solution at pH = 7 (PBS) containing 0.07 M Mo(VI) and 0.001 M Co(II). There is a range of Mo and Co concentration ratios ($\text{Mo/Co} > 20$) where the CV shows the same features and is essentially similar to that registered in solution containing no cobalt. This indicates that the charge transfer processes observed in the CV of Fig. 1 are related to electrode reactions involving only Mo. The first forward scan in cathodic direction shows two reduction waves at $E = -0.38\text{ V}$ and -0.71 V vs. SCE. The first peak could be associated with the reduction of Mo(VI) to Mo(V) (-0.38 V) [20]. The peak observed at -0.71 V , which commences at potentials of around -0.6 V , is probably associated with the reduction to Mo(IV) and simultaneous formation of a film that deactivates the electrode and causes a current drop. Thus, the CV shows peaks instead of limiting currents in spite that the electrode is rotated. At potentials more negative than -1 V the reduction current increases exponentially due to hydrogen evolution, which is visually confirmed by observation of H_2 bubbles on the electrode surface at $E < -1.2\text{ V}$ vs. SCE. The first anodic scan shows only an oxidation wave at $E = -0.68\text{ V}$ which is probably due to the re-oxidation of Mo(IV) to Mo(VI). The successive cycles of the CV show stable behaviors although the currents are smaller than those from the first cycle and the peaks are not longer defined. The modification

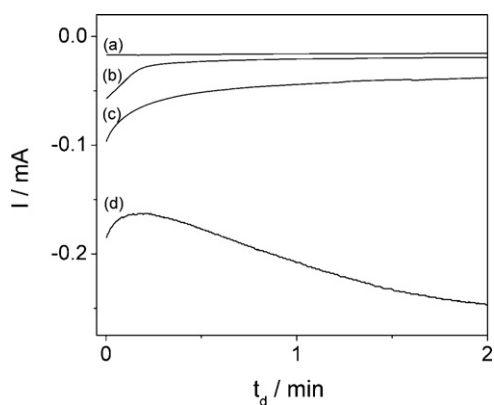


Fig. 2. Chronoamperometric curves of a polished 3-mm diameter GC RDE (1500 rpm) in 0.1 M potassium phosphate buffer (pH=7) containing 0.07 M Mo(VI) and 0.001 M Co(II). E_d (V vs. SCE) = -0.5 (a), -0.7 (b), -0.9 (c), -1.2 (d).

of the GC surface by deposition of a film is confirmed by visual examination of the electrode.

3.1.2. Potentiostatic electrodeposition

The polished GC RDE was subjected to potentiostatic steps with different deposition potential (E_d) values in the range $-1.2 \text{ V} \leq E_d$ vs. SCE $\leq -0.4 \text{ V}$ during different deposition times (t_d). These potentiostatic experiments were carried out in order to establish the potential domain where electrodeposition of a film takes place and to analyze the effect of E_d and t_d on the film properties. The resulting chronoamperometric curves obtained at selected potentials are shown in Fig. 2. A deposit is only detected (optically and by AFM) for $E_d \leq -0.6 \text{ V}$, since for larger E_d values the electrode topography resulted similar to that of a polished GC. This agrees with the deactivation observed in the CV at $E < 0.5 \text{ V}$. Thus, taking into account the electro-reduction peaks detected in the CV, it can be inferred that the deposition of the film occurs by a reduction and simultaneous precipitation of Mo(IV) species. As will be shown below, films obtained at $E_d \leq -1.3 \text{ V}$ or $t_d > 5 \text{ min}$ were not uniform. Thus, the electrodes studied in this work were prepared by potentiostatic steps using $E_d = -1.2 \text{ V}$ vs. SCE.

An issue that was analyzed in this work was the effect of thermal treatments on the film integrity and electrochemical behavior. To carry out this analysis, electrodeposited K-MoCoPO films were scraped off from the GC support and analyzed by TGA under inert atmosphere. Only a mass loss around 100°C was observed due to removal of physically absorbed water, and a less pronounced mass decay was detected upon heating up to 600°C , probably due to removal of structural water [19,21]. Based on this evidence, K-MoCoPO films deposited on GC were thermally treated at 200 , 400 and 600°C for 1 h under N_2 for further ORR evaluation.

3.2. Characterization of K-MoCoPO films

3.2.1. Morphology of the electrodeposits

The as-prepared K-MoCoPO films ($E_d = -1.2 \text{ V}$ vs. SCE, $t_d = 5 \text{ min}$) present a brownish tint and a uniform appearance along the whole RDE surface. SEM analysis indicates that these films are compact, and only minor micro-cracks and craters can be observed, as those observed in the micrograph of Fig. 3a. This morphology contrasts with that observed on films prepared using the same conditions but without cobalt in the deposition solution (Fig. 3b). The morphological features of films containing only molybdenum (K-MoPO) and of K-MoCoPO films are remarkably different. While the K-MoPO film is cracked and presents a fragmented topography typical of vitreous films such as the molybdenum oxides [20], the K-MoCoPO deposit develops as a uniform layer. On prolonged depositions ($t_d > 5 \text{ min}$)

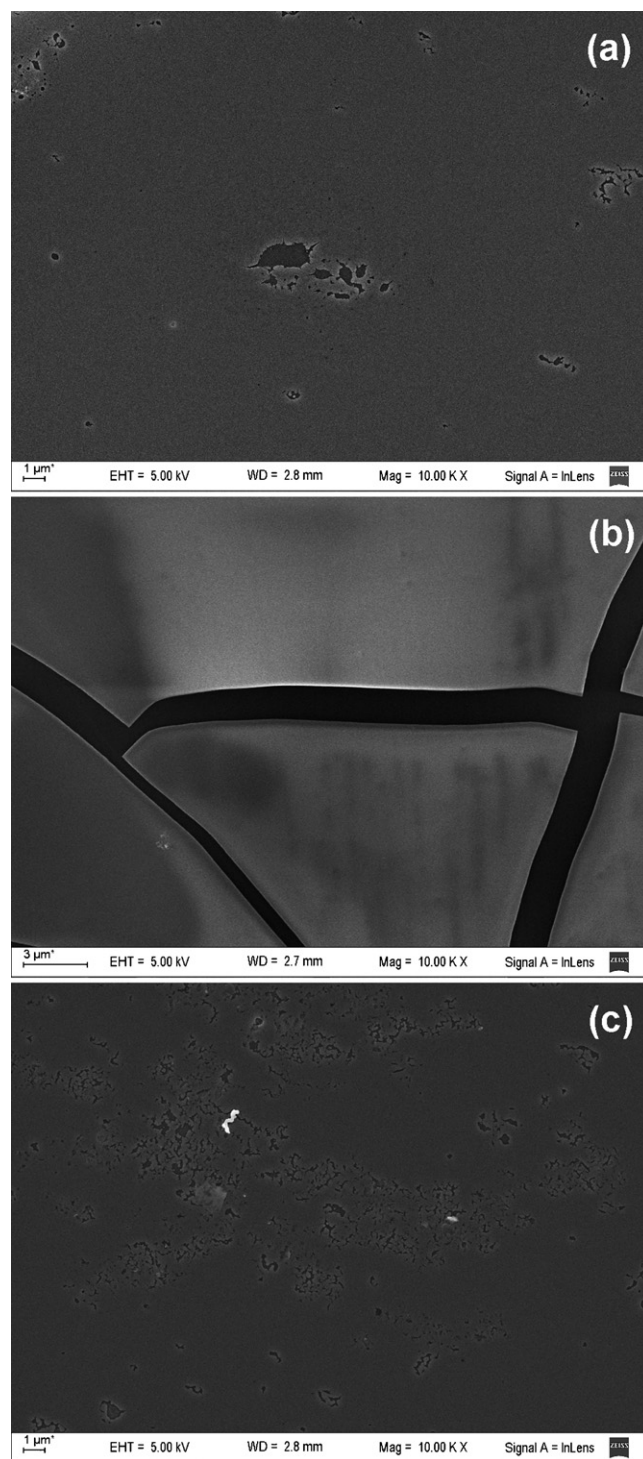


Fig. 3. SEM micrographs of: (a) Electrodeposited K-MoCoPO film on GC, $E_d = -1.2 \text{ V}$, $t_d = 5 \text{ min}$; (b) electrodeposited K-MoPO film on GC, $E_d = -1.2 \text{ V}$, $t_d = 5 \text{ min}$; (c) electrodeposited K-MoCoPO film on GC, $E_d = -1.5 \text{ V}$, $t_d = 5 \text{ min}$.

and/or very cathodic E_d values ($\leq -1.3 \text{ V}$ vs. SCE) the K-MoCoPO deposits still resulted uniform, although they presented a larger density of micropores and craters (Fig. 3c). These pores are probably formed due to gas evolution.

The film morphology at the nanometer scale is better observed in topographical and phase AFM images like those shown in Fig. 4a. It is verified that the surface is conformed by at least two phases with different morphological features. One phase grows as nanometric nodules. The other phase develops as a flat film that extends

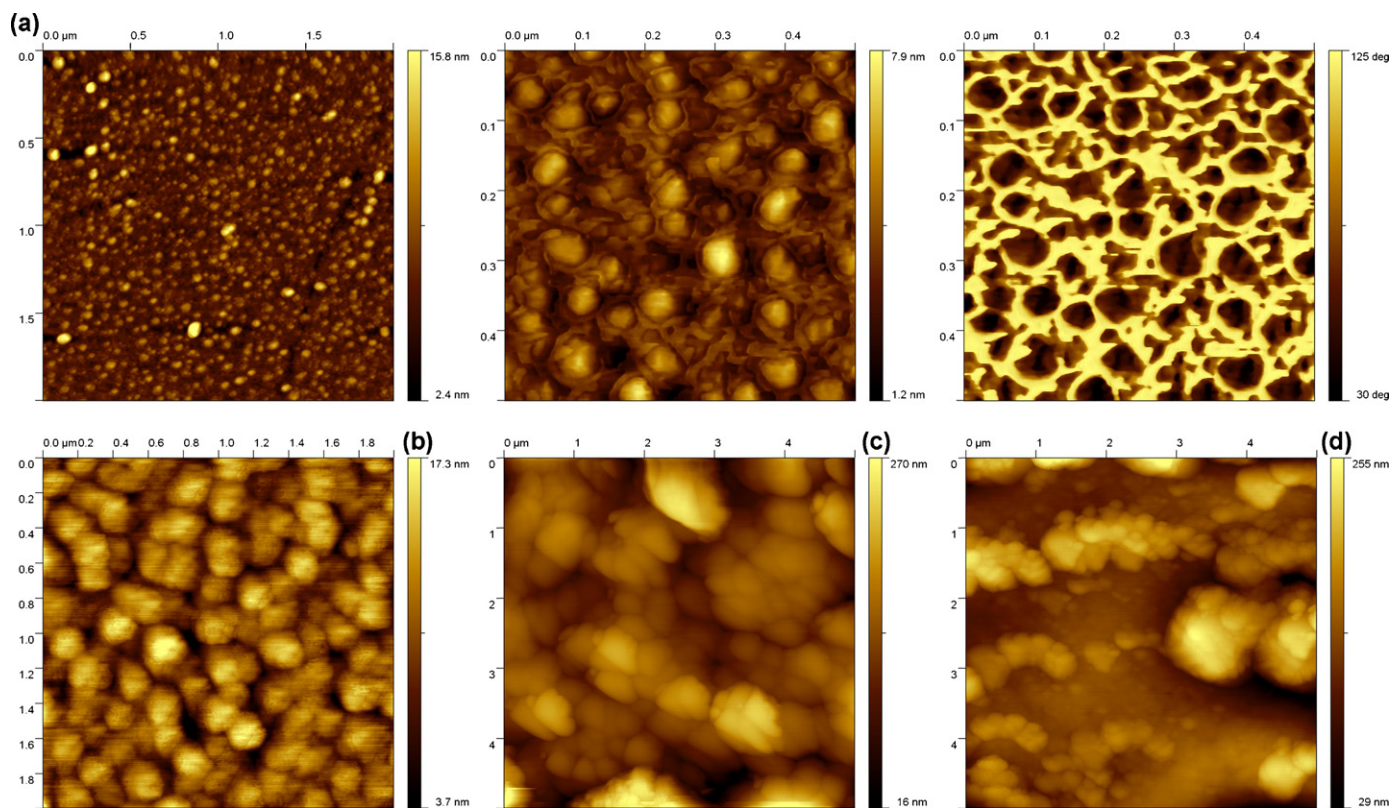


Fig. 4. Topographic and phase AFM images of a GC-supported electrodeposited K-MoCoPO film ($E_d = -1.2$ V, $t_d = 5$ min): without thermal treatment (a), thermally treated at 200 °C (b), 400 °C (c), and 600 °C (d).

over the surface surrounding the nodules and forming a grid. The AFM phase images show a strong contrast between the regions covered by the net-type layer and the rest of the surface. This indicates that this layer may be of a different chemical nature than the nodules.

Upon heating at 200 °C under inert atmosphere the film keeps its integrity. However, the AFM images (Fig. 4b) show that the sizes of the nodules are significantly larger and the existence of two phases is not longer observed. Heating at higher temperatures induces film rearrangements like those observed in Fig. 4c and d. Films that were heated at 400 °C show a very rough morphology with large particles. The film integrity collapses after heating at 600 °C.

3.2.2. Chemical characterization

EDX was used to identify elements that constitute the electrodeposits. The EDX spectra obtained on different $10 \mu\text{m} \times 10 \mu\text{m}$ regions, such as that shown in Fig. 5a, identify the $K\alpha$ lines of P, K, and Co, and the L lines of Mo. A molar P:Mo:K:Co ratio of approximately 2:3:4:1 was estimated from the EDX spectra measured on different areas. These ratios are only indicative since the film morphology and the Mo(L) line are not ideally suited to perform a quantitative EDX microanalysis.

X-ray diffraction (XRD) spectra of films electrodeposited at $E_d = -1.2$ V vs. SCE and that were scraped off from the support showed no detectable crystalline phases, even after thermal treatments at 600 °C. This indicates the presence of a disordered but stable phase. The FTIR analysis of the as-prepared material resulted in IR spectra as that shown in Fig. 5b. The observed absorption bands are broad and not very intense. These bands are located at frequency values close to those reported for a cobalt phosphomolybdate synthesized by a hydrothermal method [22]. The presence of phosphate is verified by a strong and broad band at 1050 cm^{-1} associated

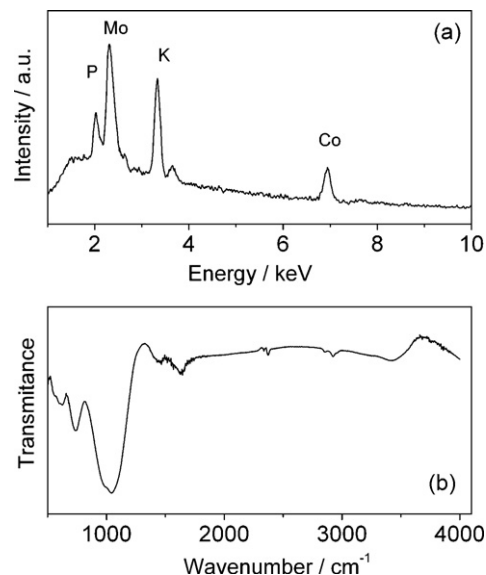


Fig. 5. (a) EDX spectra of a K-MoCoPO film electrodeposited on GC ($E_d = -1.2$ V, $t_d = 5$ min). (b) FTIR spectrum of electrodeposited K-MoCoPO ($E_d = -1.2$ V) scrapped off from the GC support.

to the $\nu(\text{P}-\text{O})$ mode. The presence of linked oxygen-coordinated molybdenum groups is verified by a partially overlapped band at 970 cm^{-1} assigned to the $\nu(\text{Mo}=\text{O})$ mode and a minor band at 730 cm^{-1} associated with the $\nu(\text{Mo}-\text{O}-\text{Mo})$. The weak bands detected in the frequency interval between 550 and 700 cm^{-1} are probably related to the $\nu(\text{Co}-\text{O})$ modes [23]. The broad band at $\sim 3500 \text{ cm}^{-1}$ can be attributed to $\nu(\text{OH})$ and $\nu(\text{HO}-\text{H} \cdots \text{O})$ modes

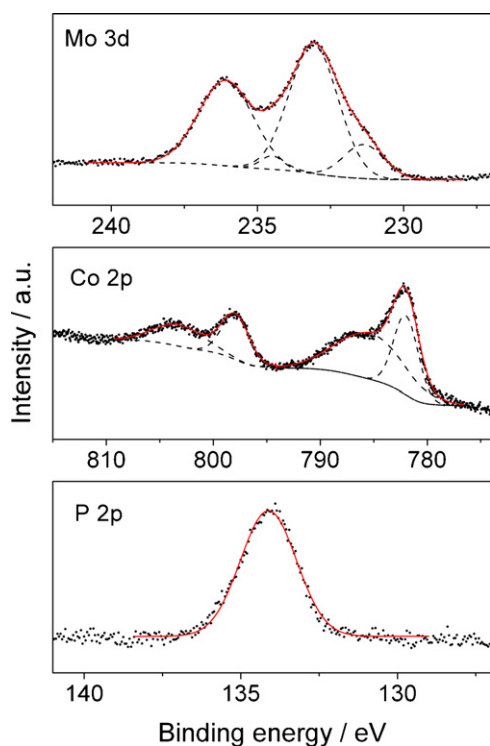


Fig. 6. Mo 3d, Co 2p and P 2p XPS spectra of a K-MoCoPO film electrodeposited on GC ($E_d = -1.2$ V, $t_d = 5$ min). Dots: experimental points; solid lines: theoretical spectra composed of peaks fitted to Gaussian functions (dashed lines).

from physically adsorbed and structural water. The IR spectra of films that were thermally treated keep these features, except by the intensities of the bands from water, which are significantly decreased. These XRD and FTIR results permit to infer that the amorphous film is composed of oxygen-coordinated molybdenum and cobalt groups linked with phosphate groups. No crystalline molybdenum or cobalt oxide phases (e.g. MoO_3 , MoO_2 , Co_2O_3 , etc.) are present in detectable amounts even after possible crystal growing by thermal treatments.

The XPS spectra measured on a K-MoCoPO film in the energy regions of Mo 3d, Co 2p and P 2p levels are shown in Fig. 6. Two pairs of signals are observed in the Mo 3d region. The two main peaks at 233.0 eV ($3d_{5/2}$) and 236.1 eV ($3d_{3/2}$) are typical of Mo(VI) [24,25]. The third peak that is detected at lower energy (231.4 eV) as a shoulder is probably due to the $3d_{5/2}$ signal of Mo in a lower oxidation state [26], most likely Mo(V) [22,24,27]. A weak fourth peak from the $3d_{3/2}$ signal of the lower-valence Mo should also show up at 234.5 eV. The Mo 3d spectra of K-MoPO and of K-MoCoPO thermally treated at 200 °C only show the first pair of signals corresponding to Mo(VI). Even though the material was deposited by electro-reduction of molybdenum, the species detected at the surface was mostly Mo(VI). This could be explained by the oxidation of the reduced molybdenum at the surface with oxygen [28] when the material was exposed to air. Notwithstanding, a fraction of Mo(V) remained in a reduced state at the film surface. The Co 2p region shows the peaks at 782 eV ($2p_{3/2}$) and 797.9 eV ($2p_{1/2}$), and their respective satellites at slightly larger binding energies, which are typical of Co(II) oxides [29]. In the P 2p region the observed line at 134.1 eV is typical of phosphates [22,25]. These results indicate the presence in the film of a small fraction of a reduced molybdenum phosphate which formation is induced by the presence of cobalt in the electrodeposition solution. This phase is thermally unstable and is not longer observed upon heating the film at 200 °C.

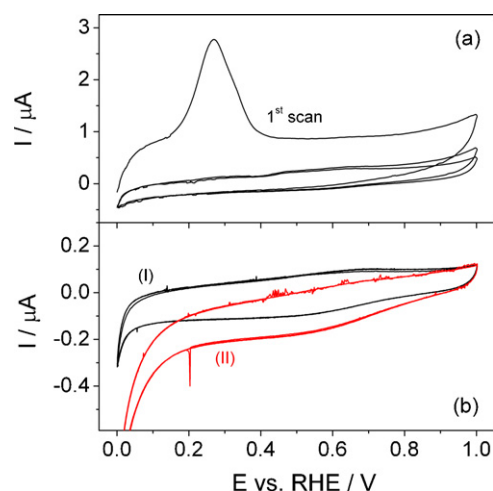


Fig. 7. (a) Cyclic voltammograms of a K-MoCoPO film electrodeposited on a GC RDE ($E_d = -1.2$ V, $t_d = 5$ min) in 0.5 M H_2SO_4 saturated with N_2 . (b) Stable CV of the same K-MoCoPO film in 0.5 M H_2SO_4 saturated with N_2 (I), and with O_2 (II). The CVs measured during the saturation with O_2 were omitted. Scan rate = 10 mV s^{-1} . $\omega = 1500$ rpm.

3.3. Oxygen reduction electrocatalysis in acid

3.3.1. Cyclic voltammetry in acid

A typical CV in N_2 -saturated 0.5 M H_2SO_4 of the as-prepared K-MoCoPO film deposited on a GC RDE (1500 rpm) is shown in Fig. 7a. The first forward scan shows an oxidation peak at 0.25 V vs. RHE, which is not observed in the following cycles. This peak is probably associated with the irreversible oxidation and dissolution of a phase containing Mo and Co. Upon continuous potential cycling the CV reaches a reproducible stable shape with features barely different to those observed on clean glassy carbon. The CVs of thermally treated films showed essentially the same features and much larger capacitive currents as an indication of larger electroactive surface areas.

As can be seen in Fig. 7b, upon saturation of the solution with O_2 the CV is shifted to more negative currents over a potential range $E < 1$ V vs. RHE. This shift is most likely associated with the reduction of dissolved oxygen on the film and indicates that this material is active for the ORR in acid. It should be noted that the cathodic currents are rather small (not larger than $0.1 \mu\text{A}$ in absolute value) over most of the potential range. An exponential increase of the current is only observed for $E < 0.3$ V vs. RHE, but the mass-transport limiting value is not reached over the analyzed potential range. The small cathodic current is independent of the film thickness. However, an early exponential increase of the current (already from $E < 0.5$ V vs. RHE) is verified on films synthesized by repetitive depositions. In this context, it is obvious that this material is still unpractical as ORR electrocatalysts. However, taking into account that this is a Pt-free material, it shows a very interesting behavior since the overpotentials ($\eta = E - E^\circ$, where $E^\circ = 1.23$ V vs. RHE) to observe ORR currents are rather small ($\eta < -0.3$ V). A deeper analysis is required to understand the origin of the small ORR currents observed at such a low overpotentials.

3.3.2. Steady-state oxygen reduction

As the potentiodynamic cathodic current observed in presence of dissolved O_2 could be caused by pseudocapacitive processes, steady state (SS) measurements were carried out. These experiments were performed in order ensure that the observed current is exclusively due to the ORR. SS polarization curves for the ORR were measured on the K-MoCoPO films in O_2 -saturated 0.5 M H_2SO_4 using potentiostatic steps. Chronoamperometric curves at constant

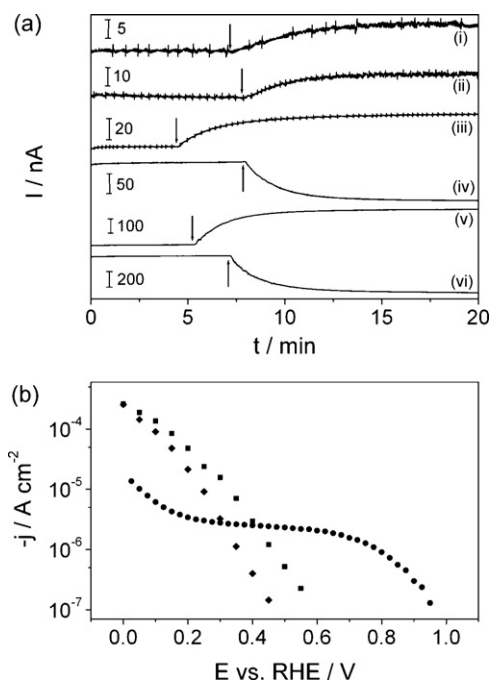


Fig. 8. (a) Chronoamperometric curves of a K-MoCoPO film electrodeposited on a GC RDE ($E_d = -1.2$ V, $t_d = 5$ min) at different potentials in 0.5 M H_2SO_4 solutions ($\omega = 1500$ rpm). Down and Up arrows indicate the point where the saturating gas was switched from O_2 to N_2 and from N_2 to O_2 , respectively. E (V vs. RHE) = 0.925 (i), 0.875 (ii), 0.8 (iii), 0.275 (iv), 0.075 (v), 0.025 (vi). (b) Steady-state ORR polarization curves measured on K-MoCoPO (circles), K-MoPO (squares) and GC (diamonds) in 0.5 M H_2SO_4 saturated with O_2 (1 atm).

potentials, such as those shown in Fig. 8a, were measured during the saturation with O_2 of a solution that was previously deaerated with N_2 , or vice versa. From these curves, the SS ORR currents at each potential were calculated as the difference between the current in O_2 -saturated solution and the current in N_2 -saturated solution. Thus, SS background-subtracted ORR polarization curves were measured in this way, which are presented in Fig. 8b. Similarly to what was observed in the CVs of Fig. 7b, SS ORR currents were detected on the K-MoCoPO film from potentials as high as 0.95 V vs. RHE ($\eta = -0.28$ V). However, upon decreasing the potential the current density seems to reach a constant limiting value much smaller than the mass-transport limiting current (j_L) and independent of the rotation rate. This could be a kinetic limiting current that is originated when a chemical reaction, i.e. the dissociative adsorption of oxygen on the active sites, is the reaction rate limiting step. This behavior was observed in recent ORR studies on platinum performed under high mass-transport conditions [30]. Notwithstanding, a limiting current density smaller than j_L and almost independent of the rotation rate can also be verified when the active sites are highly dispersed over the surface occupying a very small fraction of active area [31]. In this case the active sites behave as individual nanoelectrodes and establish a mass-transport limiting current that is defined by their sizes and surface coverage.

Fig. 8b also presents SS ORR polarization curves measured on K-MoPO films and on bare glassy carbon. These curves show that much larger overpotentials are required to obtain appreciable current for the ORR. From this point of view, the ORR response of the K-MoCoPO electrocatalyst clearly stands out from that observed on K-MoPO films.

The ORR polarization curves of K-MoCoPO films that were thermally treated (Fig. 9) indicate a strong effect of the temperature on the apparent ORR activity of the film. A thermal treatment at 200 °C modifies the film activity in a way that the ORR

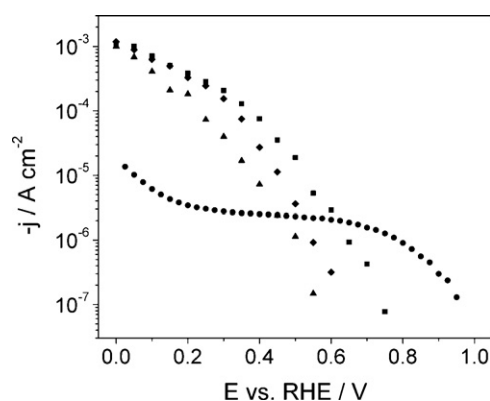


Fig. 9. Steady-state ORR polarization curves measured in 0.5 M H_2SO_4 saturated with O_2 (1 atm) on GC-supported electrodeposited K-MoCoPO as-prepared (circles), treated at 200 °C (diamonds), 400 °C (squares) and 600 °C (triangles).

overpotential increases and the limiting current is not longer observed. This result confirms that the thermal treatment causes a modification of the film chemical structure that completely changes its ORR activity. As it was detected by XPS analysis, this modification could be associated with the thermally induced transformation of the Mo(V)-containing phase. Upon increasing the temperature up to 400 °C, the overpotentials to measure significant ORR currents are slightly lower. This observation may be associated with an increase of the electroactive area as it was observed by AFM and cyclic voltammetry. The ORR activity verified on films treated at 600 °C was much lower probably due to the damage caused to the film by the heating at this high temperature.

3.3.3. Peroxide reduction

One of the main concerns associated with the operation of ORR electrocatalysts is related to the reaction products, since hydrogen peroxide can be an undesired aggressive byproduct. The quantification of the amount of H_2O_2 that is generated during the ORR is optimally carried out using a generator-collector configuration, such as the rotating ring-disk electrode [32] or the scanning electrochemical microscope [33]. However, as the sensitivity of these methods rely on collection efficiencies respect to the electrode current, in this case the collecting current should be almost undetectable. Another indirect way to obtain evidences on possible production of H_2O_2 is to test the activity of the material for H_2O_2 reduction (HPRR) [9]. The H_2O_2 generated as a product of the ORR will be reduced at the electrode surface in the potential range where the electrode is active for the HPRR. For this reason the HPRR activity of the K-MoCoPO film was evaluated in this work by cyclic voltammetry. Fig. 10 shows CVs of K-MoCoPO films in 0.5 M H_2SO_4 solutions containing different H_2O_2 concentrations. A reduction current proportional to the H_2O_2 concentration is observed over the potential range $E < 0.85$ V vs. RHE due to the reduction of H_2O_2 to water. In addition, an oxidation current with similar trend is observed from $E > 0.85$ V vs. RHE, which is most likely due to oxidation of H_2O_2 to oxygen. Thus, the mixed potential for H_2O_2 decomposition [34] is approximately 0.85 V vs. RHE. Therefore, taking into account that the reduction of H_2O_2 to water proceeds on this material for $E < 0.85$ V, water should be the product of the ORR over the whole potential range where ORR activity was observed.

3.3.4. Alcohol tolerance

Even though a systematic study of the tolerance of this material to alcohol poisoning is too premature, a quick test of ORR activity in presence of varied amounts of methanol was carried out by cyclic voltammetry. No effect of methanol in concentrations up to 0.05 M was observed on the measured ORR currents.

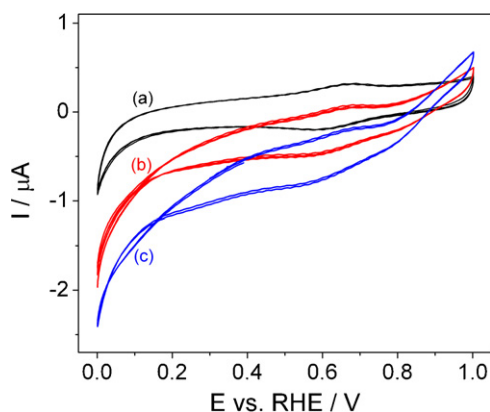


Fig. 10. Cyclic voltammograms of a K-MoCoPO film electrodeposited on a GC RDE ($E_d = -1.2$ V, $t_d = 5$ min) in 0.5 M H_2SO_4 saturated with N_2 containing 0 (a), 0.055 (b) and 0.11 (c) M H_2O_2 . Scan rate = 10 mV s^{-1} . $\omega = 1500$ rpm.

3.3.5. Film stability

The topographical and chemical properties of the films were analyzed after they were used as catalysts for the ORR in acid medium. The film can barely be detected by optical examination since it is a thin transparent coating. However, SEM analysis (Fig. 11a) permits to visualize the presence of a thin layer that shows signs of partial erosion. This layer is full of craters with dimensions ranging from the nanometers to the micrometers. The analysis by AFM (Fig. 11b) shows that at the nanoscale the film is mostly composed by a smooth thin layer that extends over the surface as a mesh. This layer was already detected by AFM on the unused film. Some isolated nanometer particles are also detected.

The analysis by EDX (Fig. 12a) revealed that most of the cobalt was removed from the film during operation in acid medium. The atomic ratios of P:Mo:K estimated by EDX were in the order of 1:2:4, indicating a dilution of P and Mo respect to the unused film. This evidence points out that a cobalt phosphomolybdate phase dissolves in acid. It is remarkable that even though most of the Co-containing phases are removed from the film, cobalt is required to obtain an active Mo-phosphate based catalyst. The analysis by XPS (Fig. 12b) indicates that at the surface these elements remain in the same oxidation state than in the untreated film, and the presence of Mo(VI) and Mo(V) can still be observed. Besides, a very weak signal is detected over the Co $2p_{3/2}$ energy range, suggesting the presence of very small amounts of this element. These results point out that the final material that was evaluated for the ORR is mostly composed by an amorphous potassium phosphomolybdate. This material is probably similar to the known polymeric structures based on anionic Mo(VI)-O clusters cohered by potassium [12,35]. However, the film also contains small amounts of Mo(V) and even smaller quantities of Co(II). These elements may be distributed either as clusters of a stable reduced molybdenum phosphate phase [22,36] or as a mixed valence phase [37].

3.3.6. Possible reasons for the observed ORR activity

The small fraction of Mo(V) and the small ORR currents observed at the lower overpotentials are two independent evidences. They indicate that the ORR proceeds at low overpotentials on Mo(V)-containing sites. Besides, films that contain only Mo(VI) such as the K-MoPO and the K-MoCoPO thermally treated presented a completely different ORR behavior. Thus, as the ORR current may be mainly limited by the low availability of these active sites, a possible way to increase the ORR performance would be to increase the fraction of Mo(V). On this sense, from the characterization of the film before and after use it is clear that the deposition process is far from being selective. At any E_d value below -0.6 V vs. SCE the catalyst layer grows by direct reduction of Mo(VI) to reduced molybdenum

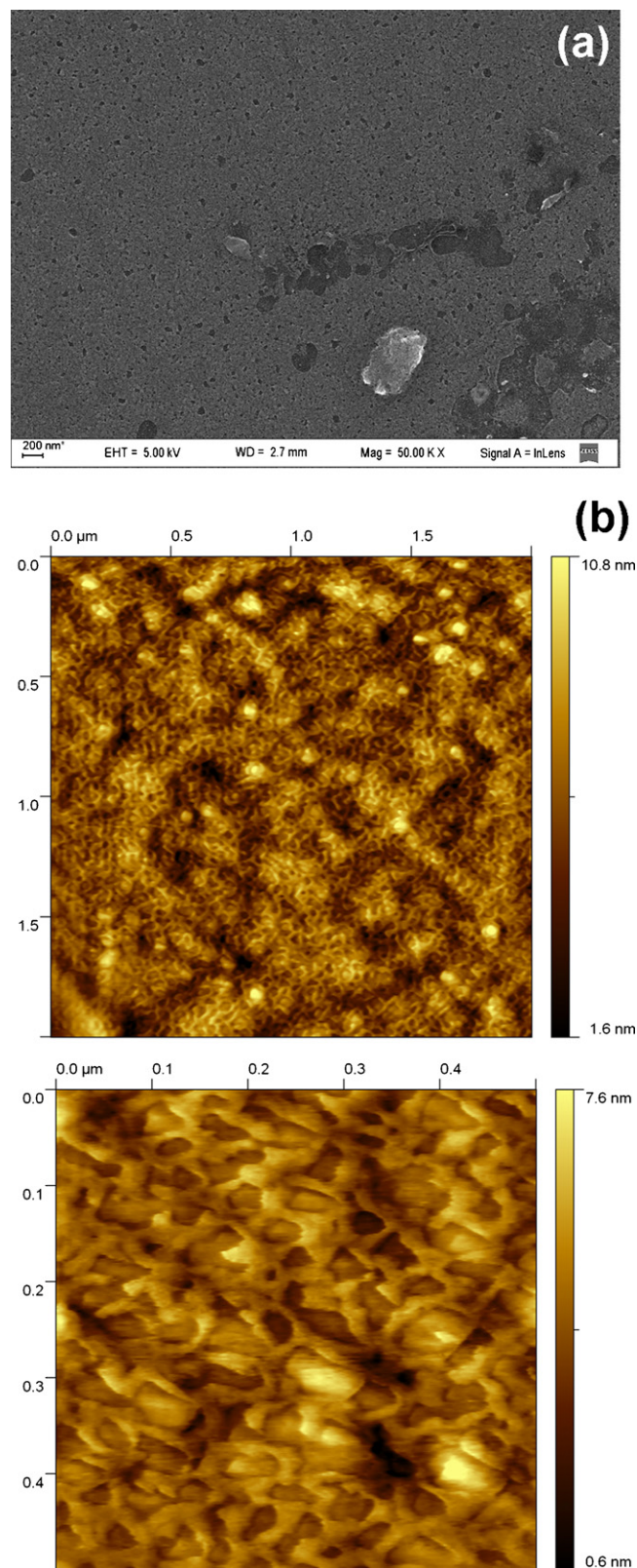


Fig. 11. SEM micrograph (a) and AFM images (b) of a K-MoCoPO film electrodeposited on GC ($E_d = -1.2$ V, $t_d = 5$ min) after ORR test in 0.5 M H_2SO_4 .

phosphate phases. However, most of this material either dissolve in acid or stay in the electrode film as re-oxidized Mo(VI)-based material. It is also possible that the deposition of species containing Mo(V) is promoted only on certain carbon surface moieties as it was previously reported [27,38]. Attempts are being made to develop a

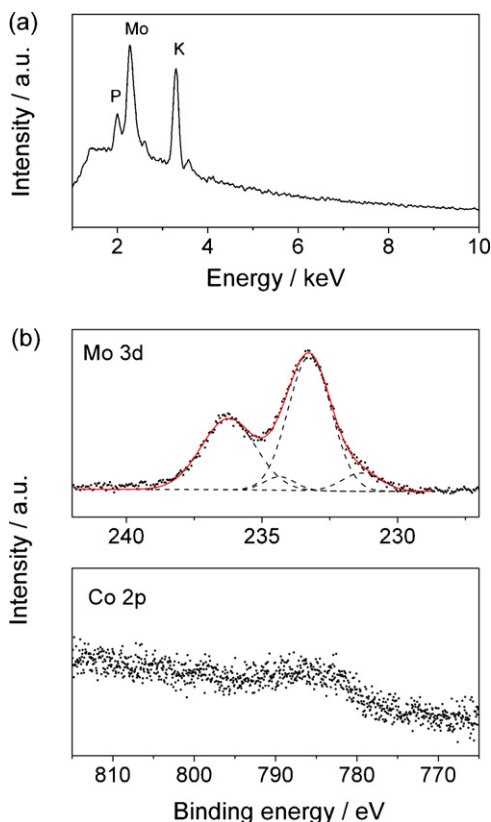


Fig. 12. EDX (a) and XPS (b) spectra of K-MoCoPO film electrodeposited on GC ($E_d = -1.2$ V, $t_d = 5$ min) after ORR test in 0.5 M H_2SO_4 . In (b) dots are experimental points and solid lines are theoretical spectra composed of peaks fitted to Gaussian functions (dashed lines).

more selective deposition method both by changing the pH of the deposition solution and by using pulsed deposition techniques.

4. Conclusions

This work demonstrates that films containing Mo(V)-based phosphates obtained by electrodeposition can function as stable and active electrocatalysts for the oxygen reduction reaction in acid media. Electrodeposition of films based on molybdenum phosphates can be carried out from potassium phosphate-containing solutions of Mo(VI) and other transition metal, for instance Co(II). The films obtained in potassium phosphate buffer at pH=7 at potentials lower than -0.6 V vs. SCE are constituted by several phosphate-based phases. Most of these phases are Mo(VI)-based compounds, presumably amorphous structures based on multinuclear Mo–O clusters polymerized via Mo–O–Mo and phosphate linkages. Some of these phases dissolve in acid. However, the most interesting and valuable fraction of the film is composed by a disperse Mo(V) phosphate phase. This phase is able to electro-reduce oxygen from overpotentials as low as -0.3 V. The amount of this active phase that is obtained by the described electrodeposition procedure is very small, so is its contribution to the total electrode current. Notwithstanding, even when the material described in this work is still unpractical, the presented study highlights the

high potentiality of these reduced molybdenum phosphates for the ORR. The key issue for future improvements is the specificity of the method used for the synthesis, which should be optimized to yield a larger amount of Mo(V)-containing phase. On this sense, the electrodeposition technique should be modified, or chemical methods such as hydrothermal synthesis could be employed.

Acknowledgements

This work was supported by Agencia Nacional de Promoción Científica y Tecnológica (ANPCyT – Argentina), Consejo Nacional de Investigaciones Científicas y Técnicas (CONICET – Argentina) and Universidad Nacional del Litoral. The assistance of M.A. Ulla in the FTIR analyses is gratefully acknowledged.

References

- [1] A.A. Gewirth, M.S. Thorum, *Inorg. Chem.* 49 (2010) 3557–3566.
- [2] J.L. Fernández, D.A. Walsh, A.J. Bard, *J. Am. Chem. Soc.* 127 (2005) 357–365.
- [3] S.L. Knupp, M.B. Vukmirovic, P. Haldar, J.A. Herron, M. Mavrikakis, R.R. Adzic, *Electrocatal.* 1 (2010) 213–223.
- [4] B. Wang, *J. Power Sources* 152 (2005) 1–15.
- [5] M. Lefèvre, E. Proietti, F. Jaouen, J.-P. Dodelet, *Science* 324 (2009) 71–74.
- [6] Q. Zhou, C.M. Li, J. Li, J. Lu, *J. Phys. Chem. C* 112 (2008) 18578–18583.
- [7] R. Jasinski, *Nature* 201 (1964) 1212–1213.
- [8] N. Alonso Vante, W. Jaefermann, H. Tributsch, W. Hönlle, K. Yvon, *J. Am. Chem. Soc.* 109 (1987) 3251–3257.
- [9] K. Itaya, N. Shoji, I. Uchida, *J. Am. Chem. Soc.* 106 (1984) 3423–3429.
- [10] R. Murugavel, A. Choudhury, M.G. Walawalkar, R. Pothiraja, C.N.R. Rao, *Chem. Rev.* 108 (2008) 3549–3655.
- [11] P.J. Bouwman, W. Dmowski, J. Stanley, G.B. Cotton, K.E. Swider-Lyons, *J. Electrochem. Soc.* 151 (2004) A1989–A1998.
- [12] M. Chojak, A. Kolary-Zurowska, R. Włodarczyk, K. Miecznikowski, K. Karnicka, B. Palys, R. Marassi, P.J. Kulesza, *Electrochim. Acta* 52 (2007) 5574–5581.
- [13] M.W. Kanan, D.G. Nocera, *Science* 321 (2008) 1072–1075.
- [14] Y. Surendranath, M. Dincă, D.G. Nocera, *J. Am. Chem. Soc.* 131 (2009) 2615–2620.
- [15] R.C. Haushalter, L.A. Mundi, *Chem. Mater.* 4 (1992) 31–48.
- [16] B. Wang, S. Dong, *J. Electroanal. Chem.* 379 (1994) 207–214.
- [17] L. Kosminsky, M. Bertotti, *J. Electroanal. Chem.* 471 (1999) 37–41.
- [18] J. Horkans, M.W. Shafer, *J. Electrochem. Soc.* 124 (1977) 1196–1202.
- [19] L. Duan, F. Liu, X. Wang, E. Wang, C. Qin, Y. Li, X. Wang, C. Hu, *J. Mol. Struct.* 705 (2004) 15–20.
- [20] R. Banica, P. Barvinschi, N. Vaszilcsin, T. Nyari, *J. Alloys Compd.* 483 (2009) 402–405.
- [21] S.E. Lister, V.J. Rixom, J.S.O. Evans, *Chem. Mater.* 22 (2010) 5279–5289.
- [22] Y. Ma, Y. Li, E. Wang, Y. Lu, X. Xu, X. Bai, *Transit. Met. Chem.* 31 (2006) 262–267.
- [23] B. Pejova, A. Isahi, M. Najdoski, I. Grozdanov, *Mater. Res. Bull.* 36 (2001) 161–170.
- [24] W. Grünert, A.Y. Stakheev, R. Feldhaus, K. Anders, E.S. Shpiro, K.M. Minachev, *J. Phys. Chem.* 95 (1991) 1323–1328.
- [25] B.V.R. Chowdari, K.L. Tan, W.T. Chia, R. Gopalakrishnan, *J. Non-cryst. Solids* 119 (1990) 95–102.
- [26] S.O. Grim, L.J. Matienzo, *Inorg. Chem.* 14 (1975) 1014–1018.
- [27] G. Ilangoan, K. Chandrasekara Pillai, *Langmuir* 13 (1997) 566–575.
- [28] E.P. Guymon, J.T. Spence, *J. Phys. Chem.* 71 (1967) 1616–1621.
- [29] B.J. Tan, K.J. Klabunde, P.M.A. Sherwood, *J. Am. Chem. Soc.* 113 (1991) 855–861.
- [30] B. Liu, A.J. Bard, *J. Phys. Chem. B* 106 (2002) 12801–12806.
- [31] C.G. Zoski, J.L. Fernández, K. Imaduwaige, D. Gunasekara, R. Vadari, *J. Electroanal. Chem.* 651 (2011) 80–93.
- [32] P.A. Christensen, A. Hamnett, *Techniques and Mechanisms in Electrochemistry*, Chapman & Hall, London, 1994.
- [33] C.M. Sánchez-Sánchez, A.J. Bard, *Anal. Chem.* 81 (2009) 8094–8100.
- [34] M. Spiro, *J. Chem. Soc., Faraday Trans. 1: Phys. Chem. Condensed Phases* 75 (1979) 1507–1512.
- [35] M.T. Pope, A. Müller, *Angew. Chem. Int. Ed.* 30 (1991) 34–48.
- [36] C. du Peloux, A. Dolbecq, P. Mialane, J. Marrot, E. Rivière, F. Sécheresse, *Angew. Chem. Int. Ed.* 40 (2001) 2455–2457.
- [37] E. Canadell, J. Provost, A. Guesdon, M.M. Borel, A. Leclaire, *Chem. Mater.* 9 (1997) 68–75.
- [38] G. Ilangoan, K. Chandrasekara Pillai, *J. Electroanal. Chem.* 431 (1997) 11–14.